A fast star sensor for balloon payloads

F. Nati, A. Benoit, P. de Bernardis, A. Iacoangeli, S. Masi, D. Yvon

10th January 2003

Abstract

We developed a system to reconstruct the attitude of balloon borne spinning experiments, where high accuracy (about 1') and high rotation speed (up to tens of degree per seconds) are required. It is based on a stellar sensor, and gathers togheter hardware simplicity, cheap components, high resolution and sensitivity. It is composed of an optical mirror (diameter 40 cm), an array of 46 fast and sensitive photodiodes, and an low noise readout electronics. It was designed for the Archeops experiment, a balloon borne millimetric telescope whose goal is to generate high resolution maps of large regions of the sky, to study the temperature anisotropies of the cosmic background radiation.

Introduction

Sky surveys by means of balloon borne telescopes are actively and effectively pursued in the microwave to infrared and UV to gamma ranges of the EM spectrum (Lee et al., 1999), (Piacentini et al., 2001), (Crill et al.,), (Devlin and the Blast collaboration, 2001), (Lamarre, 1994), (Grindlay, 1997). One of the most important and critical subsystems in these payloads is the attitude control system. This allows to control the pointing of the telescope during the flight, and allows to reconstruct it with sufficient accuracy either in real time or off-line, after the flight.

We developed a pointing reconstruction system suitable for spinning payloads, where good accuracy (about 1') despite of the high rotation speed (tens of degree per seconds) is required. It is based on a stellar sensor, with a simple and relatively cheap design. It is composed of an optical mirror (diameter 40 cm), an array of 46 fast and sensitive photodiodes, and a low noise readout electronics. This system was designed for the Archeops experiment, a balloon borne millimetric telescope whose goal is to build high resolution maps of wide regions of the microwave sky, to measure the temperature anisotropy and polarization of the cosmic microwave background (CMB) radiation (Benoît et al., 2001), (Benoit et al., 2002a), (Benoit et al., 2002b), (Benoit et al., 2002c).

Among the different attitude reconstruction systems, the star sensors are the most precise, providing a resolution which can be much better than 1' and referencing the pointing to an absolute reference frame. The main limits are size and the weight, the high data rate produced, sensitivity to daylight.

Maybe the most straightforward solution for an optical star sensor is based on a medium format CCD camera (about 500x500 pixels), but it is complex and slow to readout. This would lead to a dilution of the stars signals throughout the pixels, thus making the reconstruction quite difficult. This is why we choose a faster and simpler linear array of photodiodes at the focus of an optical telescope. The linear array is orthogonal to the scan direction. All stars with magnitude less than the limiting magnitude produce a pulse in one of the phodiodes when scanned by the array. The attitude of the payload can be reconstructed from the timing and amplitude of the pulses.

The design of the system we developed gathers together:

- hardware simplicity (both mechanical and electronics)
- cheap components
- high performances (resolution and sensitivity)
- fast, low noise readout electronics.

The disadvantage is that the system works only on scanning payloads.

1 Design and performance requirements

The detectors must be coupled with an appropriate optical telescope to achieve sufficient angular resolution and sensitivity. The angular resolution of the star sensor must be higher than the one of the millimetric telescope; for CMB work, the latter has a beam of about 8'-10'. The telescope focal plane is composed of a 46 photodiodes linear array, model Hamamatsu S4111. This

array's orientation is perpendicular to the horizon, and each pixel is 4 mm wide (azimuth or scan direction) and 1 mm high in the array direction (or cross-scan). So, for each sampling of the array, we will have 46 pixels with the same azimuth but with different elevations[1].

The mirror's focal length is determined by the angular resolution. We choose a mirror with 1.8 m of focal length, so that for the angle viewed by each pixel θ_p (in elevation) is:

$$\theta_p = \frac{d_p}{f} \simeq 1.9'$$

where d_p is the smaller pixel dimension (1 mm) and the f is the telescope focal length.

The Archeops payload continuously spins in azimuth at about 2-3 rpm; in this case the star sensor will produce a map of the sky, in one rotation period, that is 1.46° thick stripe at about 41° of elevation. The sampling period will be between 5 ms and 10 ms: in this way we have about 2-6 samples per azimuth pixel. The system must provide enough stars in each turn to maintain high accuracy of the pointing after interpolation between detected stars. From the simulations, we see that we can maintain an accuracy of about 1' in the pointing reconstruction by interpolating where stars are missing, if we have tens of stars per turn; the safe choice is a telescope that can see about 50-100 stars per turn. Using the data from the Hipparcos star catalog (ESA, 1997), we see that to achieve this, we must be able to detect magnitude 6 stars; if we can detect stars of magnitude 7 or 8, then we will have more than

[1]This is the case of the scan strategy used in Archeops. Of course, the rotation plane of the payload could be different from the azimuth plane.

100 stars per turn.

2 Implementation

2.1 Optics and sensors

2.1.1 The telescope and its mechanics

The mirror is an optical glass parabolic mirror from Meade, commercially available for optical telescopes. It has a diameter of 400 mm, and a focal length of 1830 mm. The simplest optical configuration locates the detector array at the prime focus. Since our array is quite long, we must check whether the optical aberrations of the system are smaller than the pixels.

The most distant pixel is 23 mm far from the optical axis, so the maximum off-axis angle is $\theta_{max} = arctan(23/1800)$; the most important aberrations are coma and astigmatism, respectively indicated with ASC and AAS in the following expressions (Schroeder, 1987):

$$\text{ASC} = \frac{\theta}{16F^2};\ \text{AAS} = \frac{\theta^2}{2F}$$

where F is the focal ratio. In our system we are allowed to write the following approximations:

$$coma \simeq 3F \cdot ASC = 0.15\,mm;\ astigmatism \simeq F \cdot AAS = 0.015\,mm$$

so we see that the main contribution to the aberration comes from coma, but it is still smaller than pixel dimension (1 mm).

We need to mount the read-out electronics in the same box as the photodiodes array. We have configured the box so that it covers only a small part of the mirror's area, not larger than 4%; we therefore don't need more complex solutions, i.e. with secondary mirrors, gaining simplicity and weight.

The mirror and the focal plane array are mounted on an aluminum frame. It is a very light and rigid Serrieur frame, wrapped with black velvet tissue, that prevents stray light from getting into the telescope. The frame and the tissue, inside the telescope, are both black and opaque, to minimize the internal reflections of the background light coming from sun and the residual atmosphere. On top of the telescope there is a shield that prevents stray light from reaching the photodiodes, and the sensors window has a small shield that minimizes the telescope's internal surface seen by the diodes array itself. The photodiodes box is placed on top of the telescope, with the sensors in the focus of the mirror (see Fig. 1). The focus can be adjusted by moving the support of the box, by means of two precision verniers mounted on the frame.

2.1.2 The sensor and the filter

The sensor is a linear array of 46 sensitive photodiodes (Hamamatsu model S4111 - 46Q). The array has a peak responsivity (at 960 nm) of 0.58 A/W and a dark current of 10 pA. It is sensitive in the range 190-1100 nm with a time constant of $\sim 1\mu s$ and a NEP of $2 \cdot 10^{-15} \frac{W}{\sqrt{Hz}}$. The throughput of each diode is $1.5 \cdot 10^{-7} m^2 sr$, thus we are sensitive to background variations of order of $1 \cdot 10^{-12} \frac{W}{cm^2 sr \sqrt{Hz}}$, e.g. $2 \cdot 10^{-10} \frac{W}{cm^2 sr}$ for each 5 ms sample. This can produce low frequency noise due to background variations synchronous with

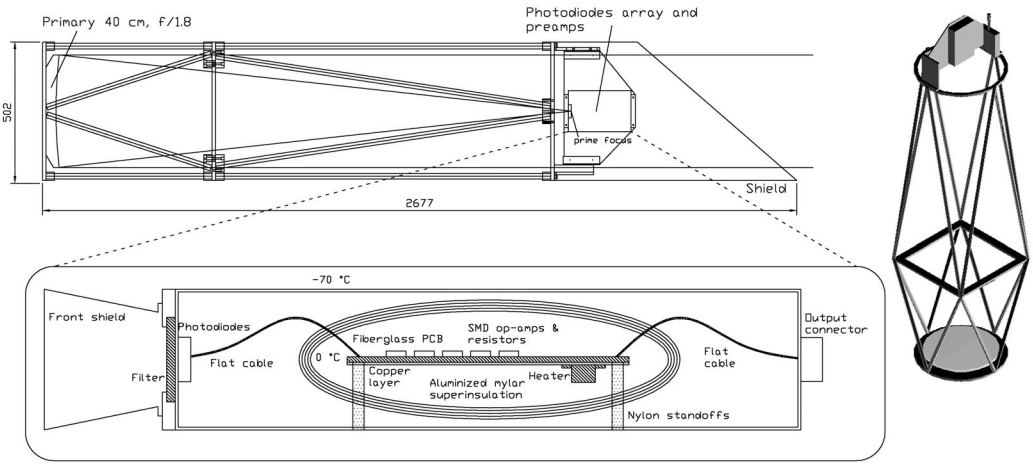

Figure 1: *Telescope frame for the star sensor a location of the various components and internal details of the photodiodes box.*

the payload rotation, especially when the Sun rises. In the Trapani flight we didn't filter the sensors: soon after dawn, the signal baseline started to oscillate, and these oscillations became soon too large to allow the detection of stars. This is due to sunlight scattered by the residual atmosphere, and to stray light that enters the telescope tube after some reflections on the balloon, on the payload and on the internal surface of the telescope. If we want to be able to see stars during the day, we need to minimize this effect. Therefore, we reduced the internal reflectivity of the telescope as much as possible (by using black non-reflecting tissue and paint), and we inserted a red filter in front of the sensors.

The aim of the filter in front of the photodiode is to cut sunlight without loosing too many stars.

We are not aware of data providing the spectrum of the blue sky in high altitude. We modeled the Sun's scattered light spectrum as the Rayleigh scattering of a blackbody spectrum with Sun's surface temperature: 5800 K.

In this model, the spectrum is strongly peaked in the ultraviolet and blue. On the other hand, the stars temperature distribution has a peak corresponding to red giants: these two considerations suggest that a low-pass filter can help to increase the signal to noise ratio. We computed the percentage of diffused light cut by the filter and the number of stars we loose, as a function of the filter's cut-on wavelength.

Hipparcos/Tycho Catalog (ESA, 1997) provide a list of stars' positions and stars' magnitudes in 4 bands. From the V-I star colors we estimated the star temperature using the temperature of the black-body of same color. We then calibrated, using measured star spectrum catalogs (Silva and Cornell, 1992), and our apparatus data, the relation

$$I_{photodiode} = f_{cal}(T_s) \cdot 10^{-\frac{m_V}{2.5}}$$

where m_V is the magnitude of the star in the V-band, and f_{cal} is the calibrated function of the star temperature. We found that using this relation, we are able to compute star magnitudes for our star sensor with an accuracy better than 0.2 magnitude, down to star temperatures of 3000 K. Selecting the 13000 brightest stars of Tycho's catalog in our target region, we find the histogram of modeled star temperature given at Fig 2.

Finally the intrinsic photodiode sensitivity versus frequency is given in Fig 3.

So as to optimize the efficiency of the star sensor, we need a tradeoff between cutting the Sun's scattered light and not loosing too many stars. We evaluated the efficiency of several optical filters to be placed in front of

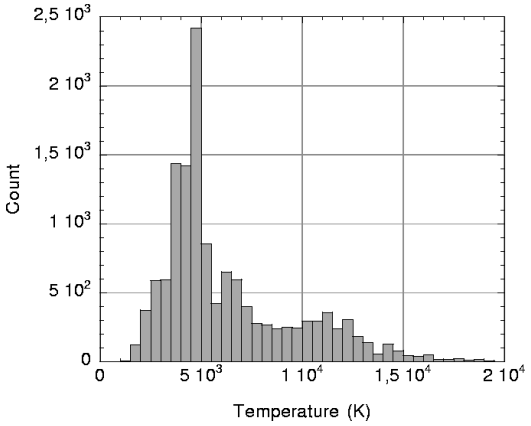

Figure 2: *Star temperature distribution of the Hipparcos/Tycho catalog. The Red giant peak is clearly seen, providing the hope that most detected stars are redder than the sky.*

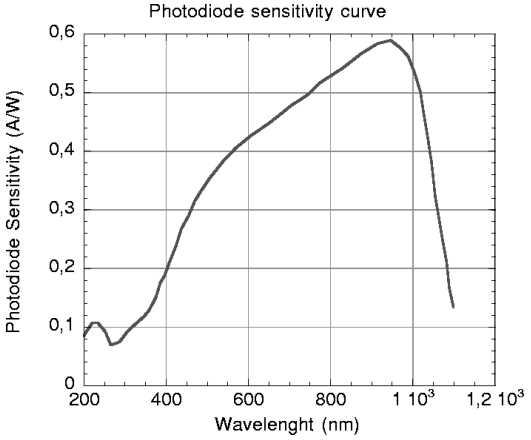

Figure 3: *Hamamatsu S4111-46Q photodiode sensitivity curve as extracted from the spec sheet. The sensitivity peaks at Red-IR wavelength.*

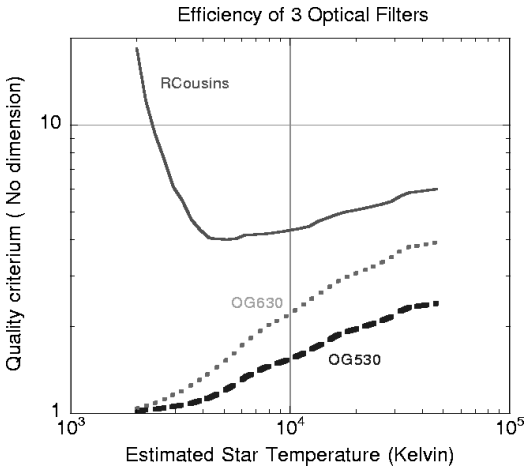

Figure 4: *This figure shows the quality factor as a function of estimated temperature for 3 of the filters we evaluated.*

the star sensor photodiode.

We define T as the modeled temperature of a star, I_{nf} the photodiode's output current without filter at a given Magnitude and I_f as the photodiode's output current using this filter at a given Magnitude. A convenient merit factor for a filter is:

$$Q(T) = \frac{I_{nf}(T)}{I_f(T)}$$

Fig. 4 shows the quality factor as a function of estimated temperature for 3 of the filters we evaluated. The closer to 1 the quality factor is, the more we detect star of this temperature.

The R Cousins filter is clearly inadequate for our use. Due to the low transmission factor (0.3) and its relatively narrow bandwidth, its cuts hard on the star flux. The expected star sensor trigger rate would drop to less than 12 candidates stars per turn.

Large bandwidth filter with high in band efficiency and sharp cutting

frequency should be preferred. We found good candidates with the OG Schott filters series. We selected two of them: the OG530 and OG630 high pass filter. Their transmission coefficient is above 0.99, with sharp transition at cutting frequency.

At Fig. 4 we plot the merit factor for the OG530 and OG630 filters. The computed quality criterium is much smaller, being close to one at the lowest star temperatures as expected.

Using the above mentioned model and datas, we computed star catalogs as seen by our apparatus using these additional filters in front of the photodiodes. Assuming a conservative threshold at the output of the photodiode, without filter, 13461 stars trigger the star detector in the target region. Using OG530 filter, 9718 stars would trigger, a 27% loss. Integrating on the modeled spectrum of the sky, we compute that the Sunlight integrated power is reduced by a factor 8.8 by the OG530 filter, but taking into account the photodiode spectral response the effective Sun light noise is cut only by a factor 3.4. If we want to achieve a rejection factor of 7 for sunlight, we have to use the OG 630 filter. The apparatus is then sensitive to 7508 stars, a loss of 44% of stars counts.

This seems the best solution, and we successfully tested the improvement during the last Archeops flight: up to 20-30 stars per turn were visible in daytime.

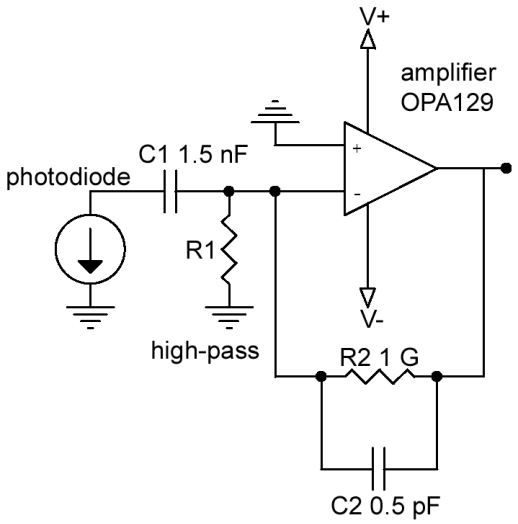

Figure 5: *Schematic of read-out electronics.*

2.2 Read-out electronics

2.2.1 Read-out schematic

The schematics of the read-out electronics is show in Fig. 5. It shows one of the array's photodiode, the RC filter and the amplification stage.

The photodiodes are used in a photovoltaic configuration for minimal noise: any bias on the photodiodes will produce high dark current, thus reducing the limit magnitude of the system. The signal from the photodiodes is AC coupled (1.06 Hz cut-on frequency in Trapani flight) to remove large scale brightness gradients. The high pass filter has a cut on frequency lower than the characteristic frequencies of the star signal, but higher than the rotation frequency of the payload. In the scan strategy used for the Archeops flights, the payload turns at 2-3 rpm, so the period is 20-30 s, while the image of a star crosses one pixel in a time given by:

$$T_s = \frac{\theta_p}{2\pi \cdot cos(\theta_{el})} \cdot P \simeq 30 - 20\text{ms}$$

where θ_{el} is the elevation angle of 41°. Therefore the characteristic frequency of the star signals is of the order of 30-50 Hz, far from both the filter and noise cut-on frequency.

The biasing resistance R_1 introduces a current noise given by:

$$I_{R_1} = \sqrt{\frac{4KT}{R_1}}$$

In the Trapani flight was $R_1 = 100M\Omega$: this is not the best choice, because this current noise is too high compared to the other contributes (see 2.2.2), from photodiodes and amplifiers. In the subsequent flights, we changed the value of R_1 to $1G\Omega$, reducing the current noise to $I_{R_1} = 3.9\frac{fA}{\sqrt{Hz}}$

The signal from photodiodes is amplified by a low noise operational amplifier (OPA129P) connected as a current to voltage converter (Fig. 5). We use a 1 GΩ feedback resistor with a 0.5 pF capacitor in parallel to get rid of gain peaking. This operational amplifier is selected because of low bias current ($I_{bias} < 100$ fA), low noise (15 $\frac{nV}{\sqrt{Hz}}$ at 10 kHz), low temperature drift (less than 10 $\mu V/C$), operating temperature in the range -40 °C to +85 °C.

2.2.2 Noise evaluation and expected total sensitivity

The purpose of this section is to evaluate the limit magnitude of the stars that can be detected by the telescope: this is important to estimate the

number of stars that can be detected in one turn.

The magnitude threshold depends mainly on the collecting area of the mirror, on the detector's noise and on the read-out noise. The power of the limit magnitude stars, collected by the mirror surface, must be higher than the total NEP of the photodiodes and of the electronics.

We now resume these main parameters of the system:

- Mirror: diameter: 0.4 m; the power collected by the mirror is given by:

$$P = \int_{A_s} F ds = \int_{A_s} \int_{\Delta_\lambda} F(\lambda) d\lambda ds$$

  where A_s is the mirror's area and Δ_λ is the optical bandwidth. To convert this power into the current produced by the photodiodes, we must make use of the responsivity of the detectors, R:

$$I = A_s \int_{\Delta_\lambda} F(\lambda) R_\lambda d\lambda$$

- Photodiodes array: from the average responsivity R_m and NEP we compute a noise current

$$I_d \simeq R_m \cdot \text{NEP} \simeq 1.2 \, \frac{fA}{\sqrt{Hz}}$$

- Read-out electronics:

1. Johnson noise (see also 2.2.1): neglecting the decoupling capacitor, R1 and R2 work as if in parallel. The resulting current noise value is : $I_{R_1} = 10 \frac{fA}{\sqrt{Hz}}$

2. OPA129 (see 2.2.1): the OPA129 contribute to the noise budget two ways: the biasing current of the Op-Amp induce a current noise $I_b = 0.1\frac{fA}{\sqrt{Hz}}$. The input voltage noise of the Op-Amp is $I_{OPA} = 0.1\frac{fA}{\sqrt{Hz}}$.

Thus the total electronics noise budget is dominated by R1 and the total noise equivalent power is $NEP_t = I_t/R_m \simeq 17\frac{fW}{\sqrt{Hz}}$. Assuming a bandwidth of 100 Hz, (sampling rate of 200 Hz), the 5 σ noise level is then given by the threshold $f_t = 1.3 \cdot 10^{-13}$ W.

The star signal is integrated over 5 ms; a magnitude $m_o = 0$ star (in the R photometric band) produces a flux $f_o = 4 \cdot 10^{-9}\frac{W}{m^2}$. If we use a mirror of 40 cm of diameter the computed threshold magnitude for a lossless system is:

$$m_l = -2.5\log(\frac{f_t}{f_o}) \simeq 8.9$$

Finally, the actual limit magnitude will be $m_l^* = m_l + 2.5\log(\epsilon)$, where ϵ is the efficiency of the whole system, including filter efficiency, reflectivity, focusing, data acquisition and star candidates extraction algorithm efficiency. Even with a total efficiency as low as 10%, the system is still able to detect magnitude 6.4.

2.3 Thermal optimization

Stratospheric flights, and in particular the arctic flights in Kiruna, present extreme temperature conditions, between -60 °C and -90 °C. We must therefore check whether the telescope's mechanics and electronics are fit for operating in such conditions.

2.3.1 Temperature effect on the telescope

When focusing the telescope on the ground, we must consider that in flight it will be at lower temperatures; this will cause the system to contract. We analyzed the differences in the thermal contractions between the telescope's frame and the focus position, due to the different materials of the mirror (glass) and of the frame (aluminum). The contraction of the focus distance is:

$$f' = f(1 + C_{glass}\Delta T)$$

where $C_{glass} \simeq 3 \cdot 10^{-6} \frac{mm}{K}$, and $\Delta T \simeq 100\ K$; so we have $\Delta f \simeq 0.54mm$. The length of the telescope will change as:

$$l' = l(1 + C_{Al}\Delta T)$$

where $C_{Al} \simeq 2 \cdot 10^{-5} \frac{mm}{K}$; therefore $\Delta l \simeq 3.6\ mm$. The mirror's $f\#$ is 4.5, so the spot becomes no more than 0.65 mm larger, that is smaller than the height of the pixel. This ensures that, even if the telescope is focused on the ground, it will remain sufficiently focused in flight.

2.3.2 Temperature control on the amplifiers

Concerning the electronics, the most critic parts in flight conditions are the operational amplifiers, since their operating temperature must not go below -40 °C. They are in the electronics box in front of the mirror, that cannot be shielded with big protections. So, for Kiruna flights, we had to miniaturize the amplifiers boards to reduce its radiative emission, and also to get enough

space inside the box to insert mylar superinsulation between the board and the box (see Fig. 1). We used the same OPA129 amplifiers in SMD package on a printed board. Besides, we used teflon supports for the two boards, and tiny diameter cables between amplifiers and the outer connectors, to minimize the thermal conductivity toward the external sides of the box. Moreover, we put a copper plate on the boards. This is an efficient ground shielding against parasitic signals and improves the thermal conductivity along the board. We mounted two heater resistances and a PT100 thermometer in contact with the copper plate to control and monitor the temperature of the boards.

Therefore, we can write the thermal balance of the board, discarding the residual atmosphere contribution:

$$W_{heater} + W_{diss} = N_{Cu}\frac{A_{Cu}}{L_{Cu}}\int_{T1}^{T2}\lambda_{Cu}(T)dT + \\ +N_{Tf}\frac{A_{Tf}}{L_{Tf}}\int_{T1}^{T2}\lambda_{Tf}(T)dT + 2A_{sk}\sigma(T_2^4 - T_1^4)F$$

where W_{heater} and W_{diss} are, respectively, the power dissipated by the heaters and by the amplifiers, $N_{Cu} \simeq 700$ is the number of cables connecting the boards to the outer connectors (each cable is actually composed of several smaller cables), $A_{Cu} \simeq 8 \cdot 10^{-3}\ mm^2$ is the cross section of such conductors, $L_{Cu} \simeq 10$ cm is their length, $T_1 \simeq$-80 °C and $T_2 \simeq 0$ °C are the external temperature and the target temperature of the circuit respectively, λ_{Cu} is the copper thermal conductivity (that is, once integrated, about $1 \cdot 10^5\ \frac{W}{m}$), N_{Tf}=4 is the number of teflon standoffs for the boards, $A_{Tf} \simeq 20\ mm^2$ is the section of such supports, $L_{Tf} \simeq 2$ cm their length, λ_{Tf} is the teflon's thermal

conductivity (its integral is about 70 $\frac{W}{m}$), $A_{sk} \simeq 100\ cm^2$ is the board's surface, $\sigma = 5.67 \cdot 10^{-8} \frac{W}{m^2 K^4}$ is the Stefan-Boltzmann constant; finally, the value of the factor F is of the order of the inverse of the number of wrapping layers of aluminized mylar around the circuits. W_{diss} is about 1 W, while the term due to the teflon support is about 0.27 W, and the two remaining terms give a contribution of 5 W each. Therefore, to maintain the temperature around, i.e., 0 °C, the power of the heaters must be at least 10 W. We used a 20 W maximum power supply, and we could successfully monitor and control the temperature of the boards during the flights, maintaining it safely inside the operating range of the amplifiers.

3 In-flight performance

The telescope has already flown six times. Once from Trapani, for the Archeops test flight in July 1999, and five times from Kiruna (one flight in April 2000, just for stellar sensor and telemetry testing, two Archeops flights in January 2001 and two Archeops flights in January and February 2002). It worked very well in all these flights, allowing the pointing reconstruction with an accuracy of very few arcminutes, and showing the improvements due to adjustments we made after each flight. Besides, it didn't required important expensive changes nor repairs, thus confirming the high reliability of the whole system.

3.1 No filter (Trapani flight)

In the first flight from Trapani (July 1999), we tested the sensors without any filter. They worked very well during the night, allowing the extraction of almost hundred star candidates per turn. The star reconstruction was easily made allowing a pointing accuracy of about 1'.

However, just after sunrise, the baseline started to oscillate, until the signal became too large, thus making star extraction impossible. This is the main problem we encountered, and our changes in the telescope design, described above, were tested in the following flights.

3.2 With filter (Kiruna flights)

The telescope with the filter and a more opaque internal surface was tested for the first time in a flight from Kiruna in April 2000, then in the four Archeops flight from Kiruna in 2001 and 2002. It worked always very well, allowing the extraction of more than hundred stars per turn during the night (see Fig. 6), and about 20-30 stars per turn during the day. The baseline oscillation during the day remained contained within the dynamical range, allowing a software filtering to flatten the signal and recognize the star peaks.

3.3 Data analysis and pointing extraction software

A separate paper will describe more details about in-flight performances and pointing reconstrucion algorithm (Benoit et al., 2002c).

Here we show a plot, on Fig. 7, of the largest amplitude star pulses, e. g.

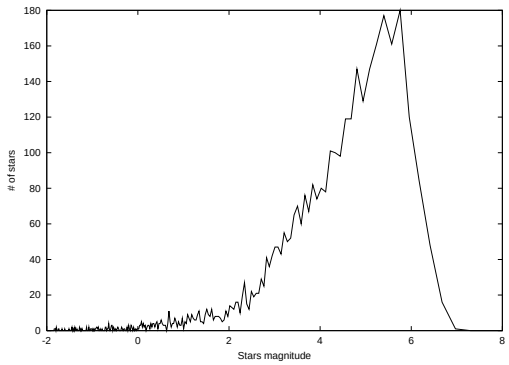

Figure 6: *Histogram of amplitudes of star candidates detected in the Kiruna flight (night).*

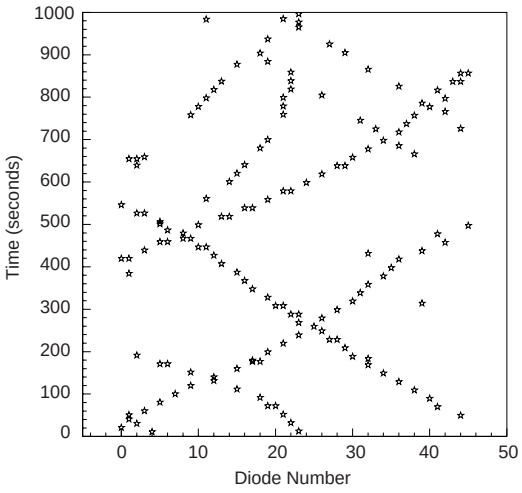

Figure 7: *This graph shows the diode number versus time of large amplitude candidate stars as seen by the stellar sensor telescope and the star detector software. Bright stars trigger the star detector every turn (20 seconds). They are seen as "tracks" in this plot: as the sky moves in front of the balloon, the star triggers move from one photodiode to the next.*

the photodiode number of candidate stars triggers versus time. Bright stars trigger the photodiodes at each rotation of the balloon over the sky. They drift over the photodiode array, as the sky drifts above the balloon.

Acknoledgement

This work has benefitted from discussions within the Archeops collaboration. We also thank J. Rich (CEA-DAPNIA, Saclay) for many discussions. The stellar sensor hardware and development has been funded by Agenzia Spaziale Italiana.

List of Figures

References

Benoit, A., Ade, P., Amblard, A., Ansari, R., Aubourg, E., Bargot, S., Bartlett, J. G., Bernard, J.-P., Bhatia, R. S., Blanchard, A., Bock, J. J., Boscaleri, A., Bouchet, F. R., Bourrachot, A., Camus, P., Couchot, F., de Bernardis, P., Delabrouille, J., Desert, F.-X., Dore, O., Douspis, M., Dumoulin, L., Dupac, X., Filliatre, P., Fosalba, P., Ganga, K., Gannaway, F., Gautier, B., Giard, M., Giraud-Heraud, Y., Gispert, R., Guglielmi, L., Hamilton, J.-C., Hanany, S., Henrot-Versille, S., Kaplan, J., Lagache, G., Lamarre, J.-M., Lange, A. E., Macias-Perez, J. F., Madet, K., Maffei, B., Magneville, C., Marrone, D. P., Masi, S., Mayet, F., Murphy, A., Naraghi, F., Nati, F., Patanchon, G., Perrin, G., Piat, M., Ponthieu, N., Prunet, S., Puget, J.-L., Renault, C., Rosset, C., Santos, D., Starobinsky, A., Strukov, I., Sudiwala, R. V., Teyssier, R., Tristram, M., Tucker, C., Vanel, J.-C., Vibert, D., Wakui, E., and Yvon, D.: 2002a, *astro-ph/astro-ph/0210305, submitted to Astronomy and Astrophysics Letter*

Benoit, A., Ade, P., Amblard, A., Ansari, R., Aubourg, E., Bargot, S., Bartlett, J. G., Bernard, J.-P., Bhatia, R. S., Blanchard, A., Bock, J. J., Boscaleri, A., Bouchet, F. R., Bourrachot, A., Camus, P., Couchot, F., de Bernardis, P., Delabrouille, J., Desert, F.-X., Dore, O., Douspis, M., Dumoulin, L., Dupac, X., Filliatre, P., Fosalba, P., Ganga, K., Gannaway, F., Gautier, B., Giard, M., Giraud-Heraud, Y., Gispert, R., Guglielmi, L., Hamilton, J.-C., Hanany, S., Henrot-Versille, S., Kaplan, J., Lagache, G., Lamarre, J.-M., Lange, A. E., Macias-Perez, J. F., Madet, K., Maffei, B., Magneville, C., Marrone, D. P., Masi, S., Mayet, F., Murphy, A.,

Naraghi, F., Nati, F., Patanchon, G., Perrin, G., Piat, M., Ponthieu, N., Prunet, S., Puget, J.-L., Renault, C., Rosset, C., Santos, D., Starobinsky, A., Strukov, I., Sudiwala, R. V., Teyssier, R., Tristram, M., Tucker, C., Vanel, J.-C., Vibert, D., Wakui, E., and Yvon, D.: 2002b, *astro-ph/astro-ph/0210306, submitted to Astronomy and Astrophysics Letter*

Benoit, A., Ade, P., Amblard, A., Ansari, R., Aubourg, E., Bargot, S., Bartlett, J. G., Bernard, J.-P., Bhatia, R. S., Blanchard, A., Bock, J. J., Boscaleri, A., Bouchet, F. R., Bourrachot, A., Camus, P., Couchot, F., de Bernardis, P., Delabrouille, J., Desert, F.-X., Dore, O., Douspis, M., Dumoulin, L., Dupac, X., Filliatre, P., Fosalba, P., Ganga, K., Gannaway, F., Gautier, B., Giard, M., Giraud-Heraud, Y., Gispert, R., Guglielmi, L., Hamilton, J.-C., Hanany, S., Henrot-Versille, S., Kaplan, J., Lagache, G., Lamarre, J.-M., Lange, A. E., Macias-Perez, J. F., Madet, K., Maffei, B., Magneville, C., Marrone, D. P., Masi, S., Mayet, F., Murphy, A., Naraghi, F., Nati, F., Patanchon, G., Perrin, G., Piat, M., Ponthieu, N., Prunet, S., Puget, J.-L., Renault, C., Rosset, C., Santos, D., Starobinsky, A., Strukov, I., Sudiwala, R. V., Teyssier, R., Tristram, M., Tucker, C., Vanel, J.-C., Vibert, D., Wakui, E., and Yvon, D.: 2002c, *paper in preparation*

Benoît, A., Ade, P., Amblard, A., Ansari, R., Aubourg, E., Bartlett, J., Bernard, J., Bhatia, R. S., Blanchard, A., Bock, J. J., Boscaleri, A., Bouchet, F. R., Bourrachot, A., Camus, P., Couchot, F., de Bernardis, P., Delabrouille, J., Desert, F. X., Dore, O., Douspis, M., Dumoulin, L., Dupac, X., Filliatre, P., Ganga, K., Gannaway, F., Gautier, B., Giard, M., Giraud-Heraud, Y., Gispert, R., Guglielmi, L., Hamilton, J. C., Hanany,

S., Henrot-Versille, S., Hristov, V. V., Kaplan, J., Lagache, G., Lamarre, J. M., Lange, A. E., Madet, K., Maffei, B., Marrone, D., Masi, S., Murphy, J. A., Naraghi, F., Nati, F., Perrin, G., Piat, M., Puget, J. L., Santos, D., Sudiwala, R. V., Vanel, J. C., Vibert, D., Wakui, E., and Yvon, D.: 2001, *astro-ph/0106152, Astroparticle Physics in press*

Crill, B., Ade, P., Artusa, D. R., Bhatia, R., Bock, J., Boscaleri, A., Cardoni, P., Church, S. E., Coble, K., deBernardis, P., deTroia, G., Farese, P., Ganga, K. M., Giacometti, M., Haynes, C. V., Hivon, E., Hristov, V., Iacoangeli, A., Jones, W., Lange, A., Martinis, L., Masi, S., Mason, P., Mauskopf, P., Miglio, L., Montroy, T., Netterfield, C., Paine, C. G., Pascale, E., Piacentini, F., Pongetti, F., Romeo, G., Ruhl, J., Scaramuzzi, F., Sforna, D., and Turner, A.

Devlin, M. and the Blast collaboration: 2001, *astro-ph/0012327*

ESA: 1997, *The Hipparcos and Tycho Catalogues, ESA SP-1200*

Grindlay, J. E.: 1997, *astro-ph/9712357 and references therein*

Lamarre, J. M.: 1994, *Infrared Phys.* **277**, 35

Lee, A. T., Ade, P., Balbi, A., Bock, J., Borrill, J., Boscaleri, A., Crill, B. P., Bernardis, P. D., Castillo, H. D., Ferreira, P., Ganga, K., Hanany, S., Hristov, V., Jaffe, A. H., Lange, A. E., Mauskopf, P., Netterfield, C. B., Oh, S., Pascale, E., Rabii, B., Richards, P. L., Ruhl, J., Smoot, G. F., and Winant, C. D.: 1999, *in 3K Cosmology, AIP 224, astro-ph/9903249*

Piacentini, F., Ade, P. A. R., Bathia, R., Bock, J. J., Boscaleri, A., Cardoni, P., Crill, B. P., de Bernardis, P., Castillo, H. D., de Troia, G., Farese, P., Giacometti, M., Hivon, E. F., Hristov, V. V., Iacoangeli, A., Lange, A. E., Masi, S., Mauskopf, P. D., Miglio, L., Netterfield, C. B., Palangio, P.,

Pascale, E., Raccanelli, A., Rao, S., Romeo, G., Ruhl, J., and Scaramuzzi, F.: 2001, *astro-ph/0105148*

Schroeder, D. J.: 1987, *Astronomical Optics*, Academic Press

Silva, D. R. and Cornell, M. E.: 1992, *ApJS* **81**, 865